from −30 to 100°C, and found that the rotational strength (independent of sign) of *all* tyrosyl side-chain transitions decreased in a gradual and similar manner with increases in temperature. Goux et al.[46] found analogous decreases in rotational strength of *all* side-chain bands with increases in temperature for the model compound α-methyl-L-tyrosine in water.
(46) W. J. Goux, D. B. Cooke, R. E. Rodriguez, and T. M. Hooker, Jr., *Biopolymers*, **13**, 2315 (1974).
(47) V. S. Ananthanarayanan, R. H. Andreatta, D. Poland, and H. A. Scheraga, *Macromolecules*, **4**, 417 (1971).
(48) S. Lifson, *Biopolymers*, **1**, 25 (1963).
(49) G. Allegra, *J. Poly. Sci., Part C*, **16**, 2815 (1967).
(50) G. W. Lehman and J. P. McTague, *J. Chem. Phys.*, **49**, 3170 (1968).
(51) All computer programs used in these calculations are available and can be obtained as directed in footnotes 26 and 27 of paper I.[16]
(52) Determined with $\sigma = 66 \times 10^{-4}$.
(53) Computed with the theory of Lifson[48] using the method outlined by Poland and Scheraga.[54]
(54) D. Poland and H. A. Scheraga, *Biopolymers*, **7**, 887 (1969).
(55) A. K. Chen and R. W. Woody, *J. Am. Chem. Soc.*, **93**, 29 (1971).
(56) For example, compare the experimental results of ref 6 and 46.
(57) A. W. Burgess, P. K. Ponnuswamy, and H. A. Scheraga, *Isr. J. Chem.*, **12**, 239 (1974).
(58) P. Y. Chou and G. D. Fasman, *Biochemistry*, **13**, 211, 222 (1974).
(59) F. R. Maxfield and H. A. Scheraga, *Biochemistry*, to be submitted.
(60) S. Tanaka and H. A. Scheraga, *Macromolecules*, **8**, 623 (1975).
(61) F. R. Maxfield and H. A. Scheraga, *Macromolecules*, **8**, 491 (1975).
(62) B. F. Erlanger and R. M. Hall, *J. Am. Chem. Soc.*, **76**, 5781 (1954).

Moments and Distribution Functions for Poly(dimethylsiloxane) Chains of Finite Length

Paul J. Flory* and Vincent W. C. Chang

Department of Chemistry, Stanford University, Stanford, California 94305.
Received August 25, 1975

ABSTRACT: The persistence vector $\mathbf{a} \equiv \langle \mathbf{r} \rangle$ and the "center-of-gravity" vector $\langle \mathbf{g} \rangle$ have been calculated for PDMS chains, both vectors being expressed in a reference frame with X axis along the initial Si–O bond and Y axis in the plane defined by this bond and the following one. The respective vectors converge with increase in chain length to the limiting persistence $\mathbf{a}_\infty$ of magnitude 7.35 Å and direction virtually coincident with the X axis. Cartesian tensors up to the sixth rank formed from the displacement vector $\boldsymbol{\rho} = \mathbf{r} - \mathbf{a}$, where $\mathbf{r}$ is the end-to-end vector for the chain of n bonds, are evaluated as the average over all configurations for n = 2–100. For $n \leq 20$, the second moment tensor $\langle \boldsymbol{\rho}\boldsymbol{\rho}^{\mathrm{T}} \rangle$ is highly asymmetric; the asymmetry decreases with n but remains appreciable, even at n = 100. Comparison of the components of the tensors of higher rank formed from the reduced vector $\tilde{\boldsymbol{\rho}} = \langle \boldsymbol{\rho}\boldsymbol{\rho}^{\mathrm{T}} \rangle^{-1/2}\boldsymbol{\rho}$ (i.e., the vector measured in the axes of the second moment ellipsoid) with the corresponding components for the freely jointed model chain establishes the equivalence of 17.0 bonds of the real chain to one of the model for $n > 50$. Spatial densities of the distribution $W_{\mathrm{a}}(\boldsymbol{\rho})$ of $\boldsymbol{\rho}$ about $\mathbf{a}$ are calculated from the three-dimensional Hermite series truncated at the term in the polynomials involving the tensor of sixth rank. The distribution is aspherical for finite n, and, unlike the polymethylene chains investigated previously, does not display cylindrical symmetry about any axis. It is negatively skewed along the direction of $\mathbf{a}$.

In order to acquire a proper appreciation of the configurational characteristics of chain molecules of a given polymer, analysis of finite sequences of units is essential. It does not suffice to consider only those parameters that characterize the chain in the limit of infinite length, e.g., the limiting moments of the chain vector $\mathbf{r}$ as embodied in the characteristic ratio $C_\infty = \lim_{n\to\infty} (\langle r^2 \rangle_0 / nl^2)$ where n is the number of bonds and l is the bond length, or the radius of gyration ratio $\langle s^2 \rangle_0 / nl^2$ in the same limit, and so on. This is implicit in the fact that the distribution function $W(\mathbf{r})$ for vector $\mathbf{r}$ invariably becomes Gaussian for an unperturbed chain of sufficient length and of finite flexibility, regardless of its chemical structure in all other respects. Hence, the single parameter $\langle r^2 \rangle_0$ characterizes the distribution function and related properties in this limit; all higher moments of $\mathbf{r}$ are then calculable from $\langle r^2 \rangle_0$. The spatial configurations of chains of various chemical structures are too diverse to be described by a single parameter. Noteworthy in this connection is the incapability of any universal model to represent faithfully the configurations of the various polymeric chains encountered in practice.[1,2] Direct analysis of each real chain is essential, without resort to artificial models equipped with adjustable parameters.

Features of the configuration peculiar to chains of a given type are manifested in full in finite sequences, typically at lengths up to about 200 skeletal bonds. Thus, for example, the ratios of moments $\langle r^4 \rangle_0 / \langle r^2 \rangle_0^2$, etc., depart markedly in this range from their values in the limit $n \to \infty$.[2-4] They reflect the structural and conformational description of the chain in question and they delineate departures of $W(\mathbf{r})$ from Gaussian.

The configurations of finite chains or of finite sequences of units in long chains, and the distribution function $W(\mathbf{r})$ describing these configurations, are matters of direct importance to x-ray and neutron scattering by high polymers in bulk and in solution at intermediate values of the magnitude of the wave vector $\kappa = (4\pi/\lambda)$ in $(\vartheta/2)$, i.e., for κ = 0.05 to 0.3.[5] The subject is relevant also to the formation of cyclic conformations within long chains; to the formation of cyclic oligomers by elimination of sequences of units, directly or indirectly, from long chains;[6-9] to the analysis of the hydrodynamic behavior of polymeric chains of any length; and to any of the physical properties of relatively short chains ($n < \sim 200$).

The finite sequence within a long chain differs from the finite chain of the same length as the sequence, owing to configurational correlations with neighboring units in the former situation. Differences arising on this account usually turn out to be small.[10,11] Hence, it is legitimate to ignore the distinction and to view results for finite chains in the broader context that includes finite sequences within long chains.

A deeper understanding of the configurations of short chains, or sequences, can be acquired by expressing the chain vector $\mathbf{r}$ and its distribution in a reference frame fixed within the chain molecule.[12-14] An internal reference frame defined by the first two bonds of the chain is a con-

venient choice for this purpose. Adoption of this basis for representation of **r** is a drastic departure from the traditional practice of employing an external reference frame within which the molecule is accorded all orientations without preference. By this artifice, the distribution $W(\mathbf{r})$ is automatically rendered spherically symmetric and the average of **r** over all configurations is made null. In the internal reference frame affixed to the first two bonds, the average of **r** is a non-null vector which we call the *persistence vector* $\mathbf{a} \equiv \langle \mathbf{r} \rangle$.[12-14] It approaches a finite limit $\mathbf{a}_\infty$ with increasing chain length. For chains of finite length, the magnitude of **a** may be substantial compared to the fluctuations of **r** about **a**.[14] These fluctuations for various configurations are expressed by the vector $\rho \equiv \mathbf{r} - \mathbf{a}$ that measures the displacement of the remote end of the chain from its average location. The Cartesian moment tensors formed from ρ and averaged over all configurations of the chain serve to characterize the spatial distribution of ρ, and hence of **r**.[13] They provide concrete information on the acentricity and anisotropy of the distribution of the remote end of the chain, and on the radial dependence of the "density" distribution of the location of the chain terminus as well.

Computations along the lines indicated have been carried out by Yoon in collaboration with one of the present authors on polymethylene chains $(CH_2-)_n$ with n = 5–200 bonds.[14] Moment tensors of second to seventh rank were computed. Approximate density distributions $W_a(\rho)$ were calculated from these moments using a three-dimensional Hermite series.[13] For $n \leq 100$ bonds, the distributions $W(\mathbf{r})$ are anistropic and appreciably skewed (negatively). For $n > 50$ bonds, the transformation that renders the ellipsoid of second moments spherical suppresses the anisotropy sufficiently to permit approximation of the *distribution thus transformed* by an equivalent, freely jointed model chain; approximately 20 actual bonds of the polymethylene chain are equivalent to one "bond" of the model.[14] (It is essential to note that this correlation with the freely jointed model does not correspond to the traditional reduction and identification of a "Kuhn segment". Displacement of the origin of coordinates to the terminus of **a** and rescaling of vector components as required to render the second moment tensor spherical are essentials of the present procedure which have no counterpart in the older scheme.)

In this paper we report results of a similar investigation of chains of poly(dimethylsiloxane), or PDMS. This chain differs from polymethylene (PM) in that its repeat unit spans two skeletal bonds instead of one. Moreover, the skeletal bond angles at Si and O differ markedly, with the result that the (preferred) planar conformation, if perpetuated, would generate a polygonal figure. Thus, unlike PM and many other polymeric chains, it does not propagate along a rectilinear axis in its planar form. The results calculated for PDMS are compared with those for PM.

Basis of the Computations

The PDMS chains under consideration are homologs of the series

$$CH_3-[Si(CH_3)_2-O-]_{x_u}Si(CH_3)_3$$

The silicon atoms at the extremities of the x_u-mer are treated as the termini of the chain comprising a linear sequence of $n = 2x_u$ bonds between these terminal atoms.

The initial portion of a PDMS chain in the planar, trans conformation is shown in Figure 1. Coordinate axes for the skeletal bonds, serially numbered in Figure 1, are defined in the conventional way.[2] That is, the axis X_i is taken along bond i; for $i > 1$ the Y_i axis lies in the plane of bonds $i - 1$ and i with its direction acute to that of the preceding bond; the Z_i axis is normal to the plane of bonds $i - 1$ and i and its direction is chosen to complete a right-handed Cartesian system. In the case of the first Si–O bond (i = 1), the preceding bond is taken to be the Me–Si bond that is trans to bond 2 in the staggered conformation of bond i;[12,13] see Figure 1. The coordinate system X_1, Y_1, Z_1 affixed to the first bond is thus defined, in fact, by skeletal bonds 1 and 2.

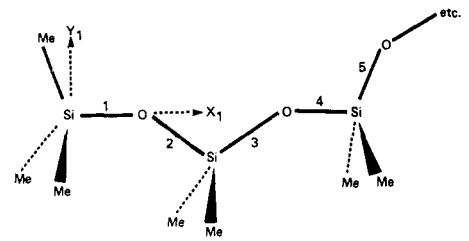

Figure 1. Initial portion of the PDMS chain in its planar trans conformation.

The length l of the Si–O bond is 1.64 Å.[15] Bond angle supplements at the O and Si atoms are taken to be $\theta_a = 37°$ and $\theta_b = 70°$, respectively.[15,16] As in previous calculations on PDMS chains,[16] the spatial configuration of the chain is conveniently treated in terms of three rotational isomeric states: trans (t), gauche-plus (g^+), and gauche-minus (g^-) located at rotations φ of 0, 120, and −120°, respectively, relative to the planar conformation shown in Figure 1. Statistical weight matrices[2,16] are

$$\mathbf{U}_a = \begin{bmatrix} 1 & \sigma & \sigma \\ 1 & \sigma & 0 \\ 1 & 0 & \sigma \end{bmatrix} \tag{1}$$

and

$$\mathbf{U}_b = \begin{bmatrix} 1 & \sigma & \sigma \\ 1 & \sigma & \sigma\omega \\ 1 & \sigma\omega & \sigma \end{bmatrix} \tag{2}$$

for the Si–O bond and for the O–Si bond, respectively. Rotational states of the bond in question are indexed on the columns in the order t, g^+, g^-; those of the preceding bond are indexed on the rows in the same order.

Treatment of the characteristic ratio of PDMS at 70°C and its temperature coefficient led to the assignments[16]

$$\sigma = \exp(-850/RT) \tag{3}$$

$$\omega = \exp(-1100/RT) \tag{4}$$

where RT is expressed in cal mol^{-1}.

With the object of affording results that may facilitate interpretation of equilibrium constants for the formation of cyclic oligomers (for which accurate experimental data are available covering a wide range of ring sizes[6]), all calculations reported below were carried out for a temperature of 110°C. At this temperature $\sigma = 0.327$ and $\omega = 0.236$ according to eq 3 and 4.

The Persistence and Mean Center-of-Gravity Vectors

Let **r** denote the chain vector defined in accordance with custom as the vector reaching from the zeroth to the n-th chain atom, i.e., it is the sum of the bond vectors $\mathbf{l}_i$ in the given configuration of the chain as a whole. Here we further specify that **r** shall be expressed in the reference frame of the first bond; see Figure 1. Then

$$\mathbf{r} = \begin{bmatrix} x \\ y \\ z \end{bmatrix}$$

where x, y, and z are the components of $\mathbf{r}$ along the axes X_1, Y_1, and Z_1. The persistence vector, being the average of $\mathbf{r}$ over all configurations of the chain, is expressed formally, therefore, by[12]

$$\mathbf{a} \equiv \langle \mathbf{r} \rangle = \begin{bmatrix} \langle x \rangle \\ \langle y \rangle \\ \langle z \rangle \end{bmatrix} \tag{5}$$

for the chain of $n = 2x_u$ bonds.

The computation of $\mathbf{a}$ from the data above, including the matrices of statistical weights given by eq 1 and 2, is readily carried out by matrix multiplication methods.[12,14,17] The generator matrices ($\mathbf{A}_i$; see ref 12, 14, 17, and 18) for $\mathbf{r}$ are first formulated from the geometrical data given above. These are then combined with the statistical weight matrices required for the computation of its configurational average $\mathbf{a}$. The methods have been described in detail previously.[17] Hence, we turn at once to the results of these computations shown in Figure 2.

The filled circles connected by the solid line in this figure represent end points of the vectors $\mathbf{a}$ for chains having the number of bonds (n) denoted by the numerals with the respective points. The component $\langle x \rangle$ is plotted on the abscissa, the component $\langle y \rangle$ on the ordinate. The PDMS chain being achiral, $\langle z \rangle$ is identically zero. Convergence to the limiting vector $\mathbf{a}_\infty$ is rapid beyond $n = 14$ bonds, or seven units; the components of $\mathbf{a}$ for $n = 32$ bonds differ from their limiting values by about 0.01%. Whereas $\langle x \rangle$ increases to its limit, 7.35 Å, with chain length, $\langle y \rangle$ decreases with n, the limiting value of $\langle y \rangle$ being only 0.16 Å. Thus, for a long chain the persistence vector in the reference frame of the first Si–O bond is directed approximately along the first bond of the chain, departing therefrom by only 1.25° in the limit $n \to \infty$. Its magnitude is 7.35_2 Å.

The foregoing results hinge on the choice of the silicon-to-oxygen bond as the first one of the sequence. If the oxygen-to-silicon bond is selected as the initial bond, we obtain $\langle x_\infty \rangle = 4.71$ Å and $\langle y_\infty \rangle = 6.95$ Å expressed in a reference frame like that for bond 2 in Figure 1. This vector of magnitude 8.40 Å makes an angle of 55.9° with the O–Si bond. The differences between the respective persistence vectors arise from the disparity of the bond angles θ_a and θ_b and the differences between the two statistical weight matrices.

The *persistence length* a_{PK} of the Porod–Kratky[19] wormlike chain may be identified with the component $\langle x_\infty \rangle$ for a simple chain, i.e., a chain having a one-bond repeat unit.[2] In a chain like PDMS having a repeat unit that spans more than one bond, a_{PK} is not uniquely defined in this manner. In the interests of resolving this ambiguity, we suppose that the persistence vectors are evaluated with reference to a bond embedded in the interior of a very long PDMS chain. Two persistence vectors corresponding to those identified above are distinguishable for the same bond depending on the chosen direction, Si–O or O–Si. Owing to effects of bond neighbors, these vectors, $\mathbf{a}_\infty'$ and $\mathbf{a}_\infty''$, may differ somewhat from those evaluated above for initial bonds of the chains. These differences are expected to be small[10,11] as noted in the introductory section. Ignoring them, we observe that $\langle r^2 \rangle_0$ for the very long chain, being the sum of $\langle \mathbf{l}_i \cdot \mathbf{l}_j \rangle$ for all bond pairs i,j, can be derived from the sum of the projections of all succeeding bonds *and* of all preceding bonds on a given bond.[2] Specifically, for very large n

$$\langle r^2 \rangle_0 = nl(\langle x_\infty' \rangle + \langle x_\infty'' \rangle - l) \tag{6}$$

where $\langle x_\infty' \rangle$ and $\langle x_\infty'' \rangle$ are the X components of the respective persistence vectors; the last term in parentheses eliminates double counting of the bond on which others are projected. Hence,

$$C_\infty \equiv \lim_{n\to\infty} \left(\frac{\langle r^2 \rangle_0}{nl^2} \right) = l^{-1}(\langle x_\infty' \rangle + \langle x_\infty'' \rangle - l) \tag{7}$$

It follows that the Porod–Kratky persistence length[19] may be identified with the mean of the respective projections on the bond; i.e., if we let

$$\bar{a}_{PK} = (\langle x_\infty' \rangle + \langle x_\infty'' \rangle)/2 \tag{8}$$

then

$$C_\infty = (2\bar{a}_{PK}/l) - 1 \tag{9}$$

which accords with the expression for a simple chain.[2]

Ignoring the difference between persistences for a terminal sequence and one embedded within a long chain, we have $\bar{a}_{PK} = 6.03$ Å according to the calculations quoted above. Substituted in eq 9, this gives $C_\infty = 6.35$, which may be compared with 6.43 calculated from the same parameters by the usual methods.[2,16] The difference reflects the errors involved in using terminal sequences instead of internal ones, as required by eq 7 and 9.

The limiting persistence vector $\mathbf{a}_\infty$ for polymethylene (PM) chains is directed at an angle of 40.2° from the first bond.[14] Its magnitude, $|\mathbf{a}_\infty| = 7.53$ Å, falls between the values 7.35 and 8.40 Å for the magnitudes of the respective vectors $\mathbf{a}_\infty$ for PDMS. Expressed as the ratios to the bond lengths, they are $|\mathbf{a}_\infty|/l = 4.92$ for PM and 4.48 and 5.12 for PDMS. On this latter basis, the acentricities of the two chains are comparable; the value for PM slightly exceeds the mean for PDMS. The persistence vector for PDMS converges with chain length (n) somewhat more rapidly than found previously for PM.[14]

A "center-of-gravity" vector $\mathbf{g}$ may be defined as follows:[13]

$$\mathbf{g} = (n+1)^{-1} \sum_{i=1}^{n} \mathbf{r}_{0i} \tag{10}$$

where $\mathbf{r}_{0i}$ is the vector from the zeroth to the ith chain atom. Thus, $\mathbf{g}$ is the mean center for all skeletal atoms, silicon and oxygen being weighted equally. Introducing the vector $\boldsymbol{\rho}_i$ defined by[12,13]

$$\boldsymbol{\rho}_i = \mathbf{r}_{0i} - \mathbf{a} \tag{11}$$

we have for the configurational average of $\mathbf{g}$

$$\langle \mathbf{g} \rangle = (n+1)^{-1} \sum_{i=0}^{n} \langle \mathbf{r}_{0i} \rangle$$

$$= \mathbf{a} + (n+1)^{-1} \sum_{i=0}^{n} \langle \boldsymbol{\rho}_i \rangle \tag{12}$$

It follows from eq 11 and the definition of $\mathbf{a}$ (see eq 5) that $\langle \boldsymbol{\rho}_i \rangle$ must vanish with increase in i. Hence, $\langle \mathbf{g} \rangle$ must converge to $\mathbf{a}_\infty$ with increase in n.[13]

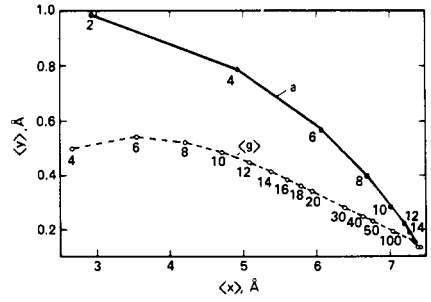

Figure 2. Persistence vector $\mathbf{a}$ (filled circles) and mean center-of-gravity vector $\langle \mathbf{g} \rangle$ (open circles) for PDMS chains having the numbers n of bonds shown by the numerals with each point.

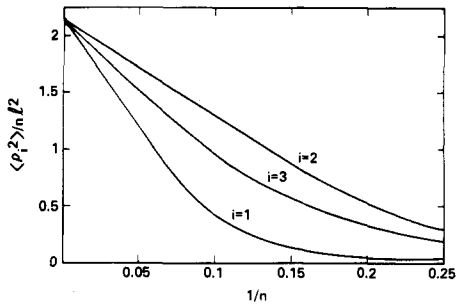

Figure 3. Principal components (see text) of the averaged second moment tensor $\langle \rho\rho^T \rangle$ plotted against the reciprocal of the chain length.

The open circles in Figure 2 represent the X and Y components of $\langle \mathbf{g} \rangle$ calculated for chains of the various lengths indicated. As expected,[14] their convergence to the limit $\langle \mathbf{g}_\infty \rangle = \mathbf{a}_\infty$ is more gradual than the convergence of $\mathbf{a}$. At $n = 100$ the vector $\langle \mathbf{g} \rangle$ differs substantially from its limit. Even at $n = 400$, the departure is preceptible, being on the order of 0.01% of the respective components according to computations not presented here in detail.

The Second Moment Tensor

In order to suppress the acentricity implicit in the persistence vector $\mathbf{a}$, it is advantageous to displace the origin of coordinates from the site of the zeroth chain atom to the terminus of $\mathbf{a}$, and to refer the location of the nth atom of the chain thereto. For this purpose, we define the displacement vector[12,13]

$$\boldsymbol{\rho} = \mathbf{r} - \mathbf{a} \tag{13}$$

The absence of subscripts will be understood to signify the full chain of n bonds ($i = n$ in eq 11). Obviously, the configurational average $\langle \rho \rangle$ vanishes.

Let the components of ρ in the reference frame $X_1Y_1Z_1$ be given by

$$\begin{aligned} u &= x - \langle x \rangle \\ v &= y - \langle y \rangle \\ w &= z - \langle z \rangle \end{aligned} \tag{14}$$

The second moment tensor formed from ρ and averaged over all configurations is

$$\langle \rho\rho^T \rangle = \begin{bmatrix} \langle u^2 \rangle & \langle uv \rangle & 0 \\ \langle uv \rangle & \langle v^2 \rangle & 0 \\ 0 & 0 & \langle w^2 \rangle \end{bmatrix} \tag{15}$$

where ρ^T is the transpose, or row form of ρ. Alternatively,[12,13] the elements of this tensor may be displayed as the column vector $\rho \otimes \rho \equiv \rho^{\times 2}$, where $\otimes$ denotes the direct product. The symbolism $\rho^{\times p}$, with $p = 2$ in this instance, is employed in the interests of simplifying the notation for tensors, or direct products, of higher rank (see below). The second moment tensor $\rho^{\times 2}$ comprises six distinct elements, two of which are null for a symmetric chain such as PDMS.

The second moment tensor is readily computed by the matrix multiplication methods presented previously.[12,13,17] Its diagonalization is achieved by rotation of the reference frame about the Z_1 axis through the angle χ defined by

$$\tan 2\chi = 2\langle uv \rangle / (\langle u^2 \rangle - \langle v^2 \rangle) \tag{16}$$

The principal components are

$$\begin{aligned} \langle \rho_1^2 \rangle &= \langle u^2 \rangle \cos^2 \chi + \langle v^2 \rangle \sin^2 \chi + 2\langle uv \rangle \sin \chi \cos \chi \\ \langle \rho_2^2 \rangle &= \langle u^2 \rangle \sin^2 \chi + \langle v^2 \rangle \cos^2 \chi - 2\langle uv \rangle \sin \chi \cos \chi \\ \langle \rho_3^2 \rangle &= \langle w^2 \rangle \end{aligned} \tag{17}$$

The principal second moments for PDMS, expressed as their ratios to nl^2, are plotted against $1/n$ in Figure 3. Computations were carried out for chains covering the range up to $n = 100$ bonds. For $n > 30$, the angle χ between ρ_1 and $\mathbf{a}$ converges to 27.9°; i.e., axis 1 is at an angle of about 27° from the persistence vector $\mathbf{a}_\infty$. In the limit $n \to \infty$, the three principal moments converge indicating the inevitable approach to spherical symmetry. The sum of the limiting ratios in Figure 3 gives the limiting characteristic ratio

$$C_\infty \equiv \lim_{n \to \infty} (\langle r^2 \rangle_0 / nl^2) = 6.43$$

in agreement with previous calculations[16] for a temperature 110°C.

For finite n, the moments decrease in the order 2, 3, 1, with $\langle \rho_1^2 \rangle$ less than one-third of $\langle \rho_2^2 \rangle$ for $n < 10$. These inequalities denote marked anisotropy in the distribution $W_a(\rho)$, which is neither spherically nor cylindrically symmetric. In the Gaussian approximation

$$W_a(\rho) = (2\pi)^{-3/2} (\langle \rho_1^2 \rangle \langle \rho_2^2 \rangle \langle \rho_3^2 \rangle)^{-1/2} \times \exp[-\tfrac{1}{2}(\rho_1^2/\langle \rho_1^2 \rangle + \rho_2^2/\langle \rho_2^2 \rangle + \rho_3^2/\langle \rho_3^2 \rangle)] \tag{18}$$

Thus, the variance is least along axis 1 and greatest along axis 2. For finite PM chains[14] the principal axis (1) nearest X is the one of least variance. However, in that case $\langle \rho_2^2 \rangle \approx \langle \rho_3^2 \rangle$ for all n. The latter observation is indicative of approximate cylindrical symmetry in PM[14] about principal axis 1.

The high degree of anisotropy indicated by the divergence of the second moments of ρ with decrease in n can be suppressed by introducing the reduced vector $\tilde{\rho}$ defined by[12,13]

$$\tilde{\rho} = \langle \rho\rho^T \rangle^{-1/2} \rho \tag{19}$$

Its components along the principal axes of the second moment tensor are

$$\tilde{\rho} = \rho_1 / \langle \rho_1^2 \rangle^{1/2}, \text{ etc.} \tag{20}$$

The ellipsoidal Gaussian distribution may then be replaced by[12,13]

$$W_a(\tilde{\rho}) = (2\pi)^{-3/2} \exp(-\tfrac{1}{2}\tilde{\rho}^T\tilde{\rho}) = (2\pi)^{-3/2} \exp[-\tfrac{1}{2}(\tilde{\rho}_1^2 + \tilde{\rho}_2^2 + \tilde{\rho}_3^2)] \tag{21}$$

which is spherical in the normalized vector space.

Higher Moment Tensors

The Cartesian tensors of higher rank are appropriately formed from the reduced vector $\tilde{\rho}$.[12-14] These tensors $\langle \tilde{\rho}^{\times p} \rangle$ were computed for $p = 3$, 4, 5, and 6 at integral values of $x_u = n/2$ throughout the range $n = 4$ to 100 bonds. Reduction of the orders of these tensors through combination of identical elements is essential in order to render the computations feasible. Methods for effecting this condensation of the tensors[20,21] and for carrying out the computations have been described.[13,17]

The moment tensor $\langle \tilde{\rho}^{\times 3} \rangle$ of third rank consists of ten distinct elements, $\langle \tilde{\rho}_1^3 \rangle$, $\langle \tilde{\rho}_1^2 \tilde{\rho}_2 \rangle$, etc., after eliminating redundances. Four of these contain odd powers of the component $\tilde{\rho}_3$ normal to the X_1Y_1 plane of symmetry. Hence, they are null for all n. The six nonzero elements of this reduced tensor are plotted against $1/n$ in Figure 4. All vanish at $1/n = 0$. Their values for finite n are indicative of skewness of the normalized distribution $W_a(\tilde{\rho})$, and hence of departures from eq 21. The 111 and 222 elements are of comparable magnitude but of opposite sign, the former being somewhat larger than the latter. Occurrence of large negative values of $\tilde{\rho}_1$ (and likewise of ρ_1) and of large positive values of $\tilde{\rho}_2$ (and of ρ_2) in excess of predictions from the

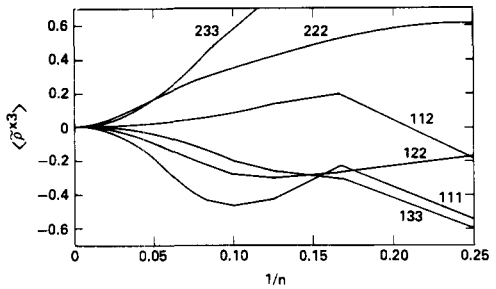

Figure 4. Elements of the tensor $\langle \tilde{\rho}^{\times 3} \rangle$ of reduced third moments plotted against $1/n$.

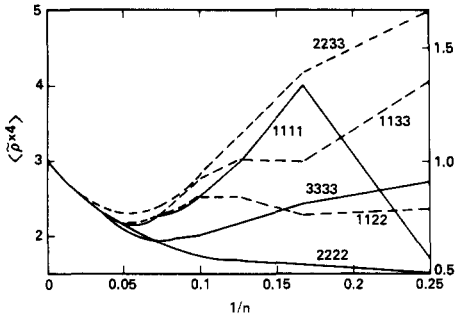

Figure 5. Even elements of the reduced fourth moment tensor $\langle \tilde{\rho}^{\times 4} \rangle$ plotted against $1/n$. The moments $\langle \tilde{\rho}_1{}^4 \rangle$, etc., shown by solid lines are referred to the ordinate scale on the left; the "mixed" moments $\langle \tilde{\rho}_1{}^2 \tilde{\rho}_2{}^2 \rangle$, etc., shown by dashed lines are referred to the scale on the right.

Gaussian distribution are indicated. These inferences are corroborated, qualitatively, by comparison of the 133 with the 233 element and of the 112 with the 122 element for $n > 10$. For smaller values of n, nonuniformities of the distribution are manifested (see below) in a more complex behavior of the moments.

The reduced tensor of fourth rank $\langle \tilde{\rho}^{\times 4} \rangle$ consists of 15 distinct elements of which the six involving odd powers of $\tilde{\rho}_3$ are null. Three of the nine nonzero elements, namely, 1112, 1222, and 1233, are small for all n and vanish as n increases. The remaining six elements are plotted aginst $1/n$ in Figure 5. Marked differences along the respective axes are apparent for short chains ($n < 20$).

Elements of the tensors of fifth and sixth ranks follow patterns resembling those for the tensors of third and fourth ranks, respectively. They are not presented here. Components of the fifth-rank tensor along the axis 1 again are negative and exceed others in magnitude, indicating greatest skewness along this axis. Elements of the tensor of sixth rank parallel the behavior of the fourth moments.

Correlation with the Freely Jointed Chain

Having suppressed the acentricity of the distribution of chain vectors **r** through the displacement of the origin by introducing vector ρ, and having diminished its anisotropy to a major degree by conversion to the normalized vector $\tilde{\rho}$, we investigate the feasibility of approximating the transformed distribution $W_a(\tilde{\rho})$ by the freely jointed or random flight model chain. Ratios of the reduced moments must conform to those for this model chain in the limit $n \to \infty$ since both the real chain and the model become Gaussian in this limit. Thus, the question raised concerns the range of chain length, commencing with very large n, over which the moments of the real chain can be approximated by the freely jointed model. Correlation of the model with the real chain requires, of course, designation of the number of real bonds that are equivalent to one step in the random flight. This ratio, which we denote by m, may be treated as an adjustable parameter.[14]

If the first bond of the freely jointed model chain may assume all orientations at random in the chosen frame of reference, then the persistence is null, $\rho = \mathbf{r}$, and all directions are equivalent. The even moments for a chain consisting of n^* bonds are given by[2,14]

$$\begin{gathered} \langle \rho_\kappa{}^2 \rangle = \tfrac{1}{3} n^* l^2 \\ \langle \rho_\kappa{}^4 \rangle = 3\langle \rho_\kappa{}^2 \rho_\lambda{}^2 \rangle = [\tfrac{1}{3} n^*(n^* - 1) + \tfrac{1}{5} n^*] l^4 \\ \langle \rho_\kappa{}^6 \rangle = 5\langle \rho_\kappa{}^4 \rho_\lambda{}^2 \rangle = 15\langle \rho_\kappa{}^2 \rho_\lambda{}^2 \rho_\mu{}^2 \rangle \\ = [\tfrac{5}{9} n^*(n^* - 1)(n^* - 2) + n^*(n^* - 1) + \tfrac{1}{7} n^*] l^6 \end{gathered} \tag{22}$$

etc., where κ, λ, and μ index the axes of an arbitrary Cartesian reference frame. Odd moments are null. Converting to reduced moments, we have[14]

$$\begin{gathered} \langle \tilde{\rho}_\kappa{}^2 \rangle = 1 \\ \tfrac{1}{3} \langle \tilde{\rho}_\kappa{}^4 \rangle = \langle \tilde{\rho}_\kappa{}^2 \tilde{\rho}_\lambda{}^2 \rangle = 1 - 2/5n^* \\ \tfrac{1}{15} \langle \tilde{\rho}_\kappa{}^6 \rangle = \tfrac{1}{3} \langle \tilde{\rho}_\kappa{}^4 \tilde{\rho}_\lambda{}^2 \rangle = \langle \tilde{\rho}_\kappa{}^2 \tilde{\rho}_\lambda{}^2 \tilde{\rho}_\mu{}^2 \rangle \\ = 1 - 6/5n^* + 16/35n^{*2} \end{gathered} \tag{23}$$

etc. Terms beyond the first in these polynomials reflect departures from the Gaussian distribution in three dimensions.

Suppression of the persistence vector through adoption of the premise that the first bond, like succeeding bonds, may orient freely (which is tantamount to adoption of an external reference frame) introduces an element of incompatibility with the foregoing treatment of the real chain referred to an internal coordinate system. In quest of a means of circumventing this minor difficulty, we note that if correlations between bonds of the real chain were relaxed, then in the limit of vanishing correlations only the first bond would contribute to the persistence. Accordingly, it seems appropriate to disregard the first bond of the real chain in seeking to establish correlation with the model. On this admittedly arbitrary basis[14] we equate each bond of the model to m bonds *beyond the first* of the real chain, i.e., we let

$$n^* = (n - 1)/m \tag{24}$$

Use of the relationship $n^* = n/m$ in place of eq 24 would not materially affect the results to follow.

Introducing eq 24 into 23, we obtain

$$\langle \tilde{\rho}_\kappa{}^2 \tilde{\rho}_\lambda{}^2 \rangle_0 - \langle \tilde{\rho}_\kappa{}^2 \tilde{\rho}_\lambda{}^2 \rangle_{\text{equiv}} = K_{\kappa\lambda} m/(n - 1) \tag{25}$$

and

$$\langle \tilde{\rho}_\kappa{}^2 \tilde{\rho}_\lambda{}^2 \tilde{\rho}_\mu{}^2 \rangle_0 - \langle \tilde{\rho}_\kappa{}^2 \tilde{\rho}_\lambda{}^2 \tilde{\rho}_\mu{}^2 \rangle_{\text{equiv}} = K_{\kappa\lambda\mu}[m/(n - 1)][1 - 8m/21(n - 1)] \tag{26}$$

where the subscript "0" denotes the moment in the limit $n \to \infty$, and the subscript "equiv" denotes the model chain of n^* bonds. It follows from eq 23 that the constant $K_{\kappa\lambda}$ assumes the value $\frac{6}{5}$ for $\kappa = \lambda$ and $\frac{2}{5}$ for $\kappa \neq \lambda$. Similarly, $K_{\kappa\lambda\mu}$ assumes values of 18, $\frac{18}{5}$, and $\frac{6}{5}$ for $\kappa = \lambda = \mu$, $\kappa = \lambda \neq \mu$, and $\kappa \neq \lambda \neq \mu \neq \kappa$, respectively.[14]

If the reduced moment for the real chain converges to that of the model chain as n increases, then the difference between the limiting value of the reduced moment and its value for the real chain of length n should approach eq 25, or 26, as n increases. In order to put this conjecture to test, these differences multiplied by $n - 1$ and divided by the appropriate constant K are plotted against $1/(n - 1)$ in Figures 6 and 7. The former figure shows representative even fourth moments treated in this manner; the latter shows representative even moments of the sixth rank. It

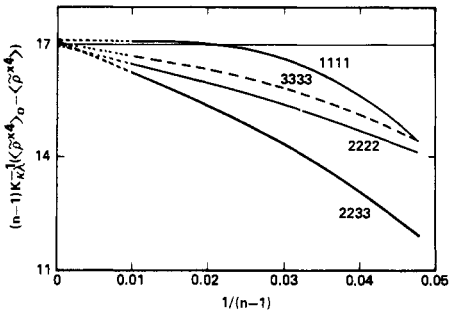

Figure 6. Differences between representative elements of the fourth moment tensor (reached at $n = \infty$) and their values for the finite chain of length n, this difference being multiplied by $n - 1$, divided by the appropriate constant $K_{\kappa\lambda}$ (see eq 25), and plotted against $1/(n - 1)$. The horizontal line represents the freely jointed chain scaled with $m = 17.0$.

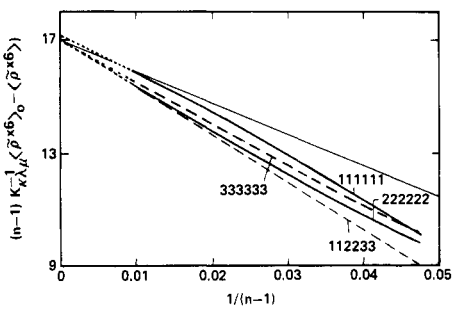

Figure 7. Plot of sixth moment differences in the manner of Figure 6; see eq 26. The solid straight line represents the freely jointed chain scaled with $m = 17.0$.

will be apparent from eq 25 and 26 that the intercepts give directly the limiting values of m for the respective moments.

The intercepts for the six even fourth moments, four of which are presented in Figure 6, fall within the range m = 16.97 to 17.09. Those for the ten even sixth moments, four of which are included in Figure 7, are in the range m = 16.85 to 17.16. Thus, all of the even fourth moments and all of the even sixth moments point to virtually the same value for the equivalence ratio m; approximately 17 real bonds correspond to one bond of the "equivalent" freely jointed model.

The horizontal straight line in Figure 6 represents eq 25 with $m = 17.00$; the straight line in Figure 7 represents eq 26 for the same value of m. The results for the real chains conform fairly well to these lines for $n > 50$ bonds. Even at $n = 40$ bonds (only 2.35 equivalent bonds!) the model reproduces the departures of the reduced fourth moments from their limiting values with an error of only 14% in the worst case. For the sixth moments, the model with m = 17.0 reproduces the corresponding departures from limiting values of the reduced moments with an error that does not exceed 10%.

All of the odd moments for PDMS are very small for chains with $n > 40$; they are commensurate with the departures from the straight lines representing the model chains in Figures 6 and 7. It follows that the freely jointed model with $m = 17.0$ succeeds in approximating *all* moments, at least up to and including those of sixth rank, for chains in this range.

If this measure of agreement holds for moments of higher rank, then it must follow that the distribution function $W(\mathbf{r})$ may be estimated from that for the freely jointed chain of equivalent length as dictated by the parameter m = 17.0. Specifically, the distribution for the equivalent

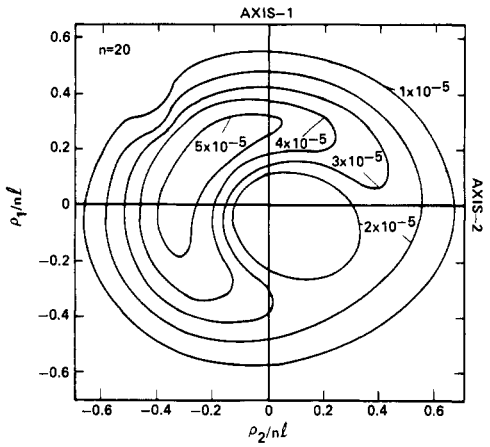

Figure 8. The density distribution function $W_a(\rho)$ of ρ in the plane of principal axes 1 and 2 of the second moment tensor for the PDMS chain with $n = 20$. The curves represent contours of constant density as calculated from the three-dimensional Hermite series, eq 27, truncated at $\nu = 6$. The densities are expressed in Å^{-3} in the space of the displacement vector ρ.

chain *of integral* n^* may be computed from the Rayleigh integral expression for $W(\mathbf{r})$.[2] This distribution should then be transformed by the inverse of the normalization operation. Finally, the origin of coordinates must be restored to the zeroth atom of the chain through the displacement $-\mathbf{a}$. The Rayleigh equation applies only for integral values of n^*. The procedure is limited on this account.

The conversion factor for PM chains,[14] $m = 20 \pm 1$, is somewhat greater than for PDMS. Values of m indicated by the various fourth and sixth moments of PM are distributed over a wider range than for PDMS. The difference between m values implies that PDMS is a somewhat more tortuous chain, a characteristic often identified with "flexibility".

Density Distributions Functions

The density distribution for vector ρ about the terminus of the persistence **a** can be expanded about the Gaussian function in a three-dimensional Hermite series as follows[13]

$$W_a(\rho) = (2\pi)^{-3/2}(\det\langle\rho\rho^T\rangle)^{-1/2}\exp(-\tfrac{1}{2}\tilde{\rho}^2)\times\left[1 + \sum_{\nu=3}^{\infty}(\nu!)^{-1}\langle\mathbf{H}_\nu\rangle\cdot\mathbf{H}_\nu(\tilde{\rho})\right] \quad (27)$$

where $\mathbf{H}_\nu(\tilde{\rho})$ is the polynomial, defined elsewhere,[13] in the tensors of rank ν, $\nu - 2, \ldots$, and $\langle\mathbf{H}_\nu\rangle$ is its average over all configurations; the dot denotes their inner product; $\tilde{\rho}$ is related to ρ according to eq 19; $W_a(\rho)$ is normalized to unit range in ρ. Thus, the coefficients $\langle\mathbf{H}_\nu\rangle$ are functions of $\langle\tilde{\rho}^{\times\nu}\rangle$, $\langle\tilde{\rho}^{\times(\nu-2)}\rangle$, etc. The coefficients up to and including $\langle\mathbf{H}_6\rangle$ were evaluated from the moments discussed above.

The densities $W_a(\rho)$ were calculated in the planes defined by each of the three pairs of principal axes of ρ for PDMS chains with n = 10, 20, 40, and 100 bonds. All calculations were carried out according to eq 27 truncated at ν = 6. Results for $n = 20$ are shown in Figures 8, 9, and 10, where contours of equal density, expressed in Å^{-3}, are plotted over coordinates expressed as ρ_i/nl. Symmetry with respect to the $\rho_1\rho_2$ plane is of course dictated by the chain structure. That the density distribution is markedly nonspherical is at once apparent. Examination of the three plots in combination confirms the absence of vestiges of cylindrical symmetry, as inferred above from the moments. The maximum is displaced appreciably from the origin; it lies between the positive axis 1 and negative axis 2, and is centered at $\rho_3 \equiv z = 0$. A minimum occurs on the opposite

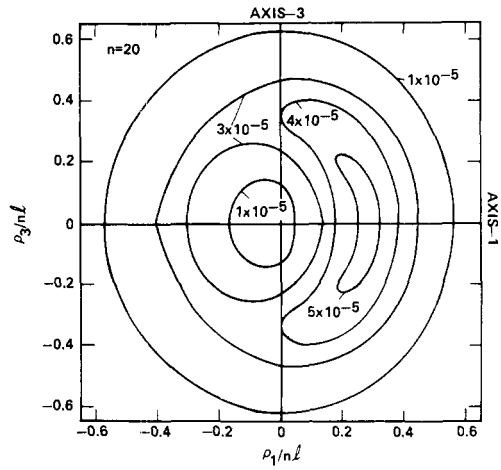

Figure 9. The density distribution $W_a(\rho)$ for $n = 20$ in the plane of axes 1 and 3. See legend for Figure 8.

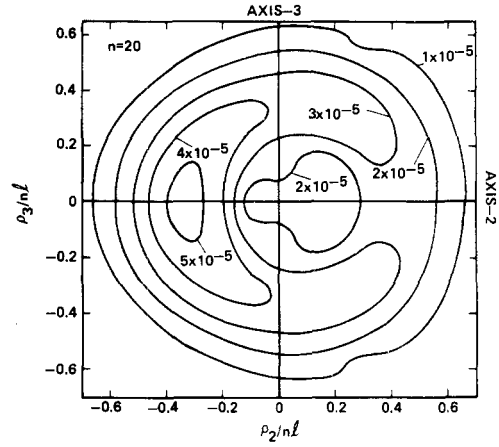

Figure 10. The density distribution $W_a(\rho)$ for $n = 20$ in the plane of axes 2 and 3. See legend for Figure 8.

side of the origin, but is much closer to the origin than is the maximum.

In Figure 11 the densities along each of the three principal axes are plotted against ρ_κ/nl. A major maximum occurs along axis 1 at $\rho_1/nl \approx 0.25$, a minimum at ca. −0.05, and a second maximum at ca. −0.35. Along axis 2 the corresponding features occur approximately at $\rho_2/nl = -0.35$, 0.05 and 0.4. The maxima along axis 3 occur at $\rho_3/nl \approx \pm 0.35$. These values do not locate the actual maxima and minimum, as will be apparent from Figure 8–10 and the discussion above. The negative value of the calculated density at the minimum is an indication of the insufficiency of the Hermite series for short chains when it is truncated at $\nu = 6$. Whereas the quantitative accuracy of the truncated moment expansion is obviously deficient, we are of the opinion that it can be relied upon to reproduce qualitative characteristics of the distribution. This matter has been discussed in greater detail previously.[14]

In Figure 12 we show the densities $W(\mathbf{r})$ for $n = 20$ along the principal axes 1, 2, and 3 of ρ, the displacements being measured from $\mathbf{r} = 0$. The curves represent sections of the same density distribution that is represented in Figures 8–10, but with the origin shifted to the starting point of the chain; i.e., the origin is displaced by the components of $-\mathbf{a}$. Since $\mathbf{a}$ is at an angle of ca. 27° from axis 1 (see above), the greatest displacement occurs along this axis (compare Figure 11). Shown for comparison is the spherically symmetric Gaussian distribution for the same value of $\langle r^2 \rangle_0$.

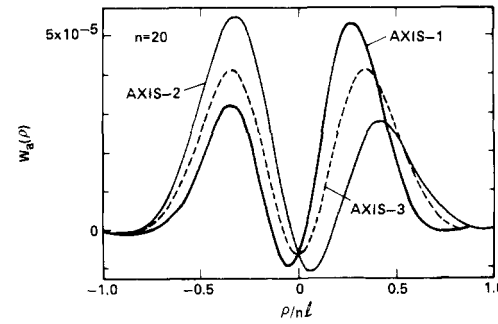

Figure 11. Densities $W_a(\rho)$ in Å^{-3} along each of the principal axes of the second moment tensor $\langle \rho\rho^T \rangle$, for $n = 20$.

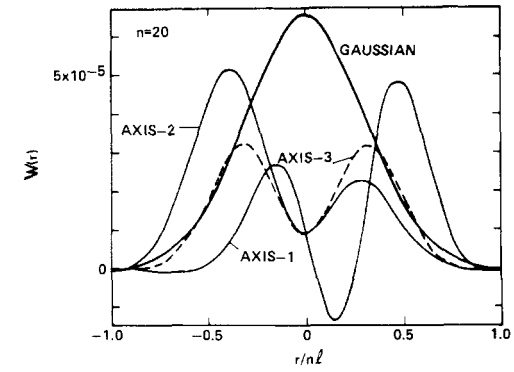

Figure 12. The density distribution $W(\mathbf{r})$ of chain vector $\mathbf{r}$ for $n = 20$ along each of the principal axes of $\langle \rho\rho^T \rangle$ with origin at $\mathbf{r} = 0$. Densities in Å^{-3}. The spherically symmetric Gaussian distribution is shown for comparison.

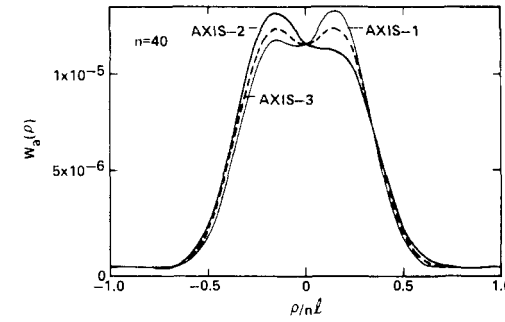

Figure 13. The density distribution $W(\mathbf{r})$ along principal axes 1, 2, and 3 for $n = 40$. See legend for Figure 12.

Densities $W_a(\rho)$ calculated for $n = 40$ and plotted as in Figures 8–10, but not reproduced here, again reveal a minimum near the origin ($\rho = 0$). It is much less pronounced, however. Each of the two maxima is situated closer to the origin, and the density contours are more nearly circular. Densities along each of the three axes are shown in Figure 13. Comparison with Figure 11 demonstrates the marked decrease in asymmetry about $\rho = 0$ with this twofold increase in n.

The density $W(0)$ at $\mathbf{r} = 0$, where the error of the Gaussian distribution is large for short chains,[14] is examined in Figure 14. Values of $W(0)$ were computed according to eq 27 truncated at successive values of ν from two to six as indicated in the figure. The ordinate represents $W(0)$ thus calculated relative to the density of the spherically symmetric Gaussian at $\mathbf{r} = 0$. For short chains, the Gaussian function grossly overestimates the density at the origin. The Hermite series shows evidence of reasonable conver-

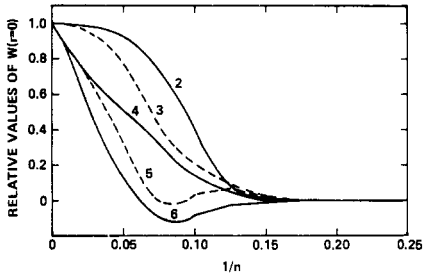

Figure 14. Densities $W(\mathbf{0})$ at $\mathbf{r} = 0$ calculated according to eq 27 truncated at the values of ν indicated, with each curve plotted against $1/n$.

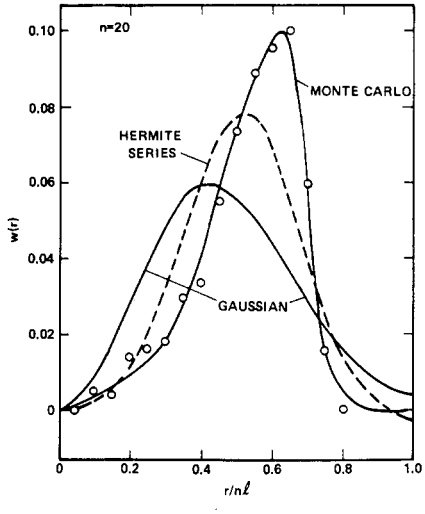

Figure 15. Radial distributions $w(r)$ in Å^{-1} for PDMS with n = 20. The dashed curve is calculated from the Hermite series (eq 27) truncated at $\nu = 6$. Open circles and the associated curve represent results for 5000 Monte Carlo configurations generated using conditional probabilities evaluated from eq 1 to 4. The lowermost curve represents the spherically symmetric Gaussian having the same second moment, $\langle r^2 \rangle_0$.

gence (at $\mathbf{r} = \mathbf{0}$) only for $n > 40$. These findings closely follow those for PM.[14]

The Radial Distribution

Radial distributions $w(r)$, representing the incidence of values of r per unit range in r irrespective of direction, were evaluated by numerical integration of the computed values of $W_a(\rho)$ for $\rho = \mathbf{r} - \mathbf{a}$ over all directions $\mathbf{r}$ with $|\mathbf{r}| = r$. They are compared with spherical Gaussians centered at $\mathbf{r} = \mathbf{0}$ in Figures 15 and 16 for $n = 20$ and 40, respectively. Departures from the Gaussian for $n = 40$ (Figure 16), though substantial, are much less than those for n = 20 (Figure 15).

Whereas evaluation of the density distribution in three dimensions by Monte Carlo methods is impracticable, the radial distribution is readily amenable to estimation in this manner. Monte Carlo chains were generated from conditional probabilities derived from the statistical weight matrices (see eq 1 and 2) using the parameters given above. Details of the procedure have been given previously.[14] The points shown in each of the two Figures, 15 and 16, represent results for sets of 5000 chains generated in this manner. The intervals chosen will be apparent from the spacing between adjacent points.

If we accept the curves through the points from the

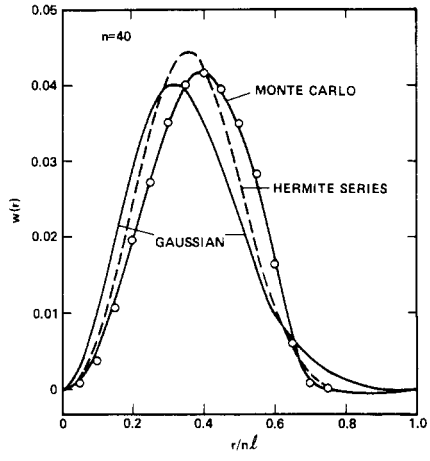

Figure 16. Radial distributions $w(r)$ in Å^{-1} for $n = 40$. See legend for Figure 15.

Monte Carlo calculations as representative of the actual radial distributions (within limits of statistical error in the points), then the differences between the Gaussian and Hermite ($\nu = 6$) curves are almost as great as the differences between the latter and the actual distribution. The Hermite series truncated at $\nu = 6$ nevertheless affords an acceptable approximation to the actual distribution for n ≥ 40. The detail afforded by the Hermite series computation of the density in three-dimensional space is suppressed in the integration over all direction to obtain the radial distribution. Hence, the comparisons in Figures 15 and 16 are offered primarily as evidence bearing on the efficacy of the truncated Hermite series. While inaccurate quantitatively, it affords a substantial improvement over the Gaussian distribution and should therefore serve its intended purpose of portraying the principal features of the density distribution in three dimensions.

Acknowledgment. This work was supported by the National Science Foundation, Grant No. DMR-73-07655 A01.

References and Notes

(1) T. M. Birshtein, *Vysokomol. Soedin., Ser. A*, **16**, 54 (1974).
(2) P. J. Flory, "Statistical Mechanics of Chain Molecules", Interscience, New York, N.Y., 1969.
(3) R. L. Jernigan and P. J. Flory, *J. Chem. Phys.*, **50**, 4178 (1969); P. J. Flory and R. L. Jernigan, *ibid.*, **42**, 3509 (1965).
(4) K. Nagai, *J. Chem. Phys.*, **48**, 5646 (1968).
(5) D. Y. Yoon and P. J. Flory, *Polymer*, **16**, 645 (1975).
(6) P. J. Flory and J. A. Semlyen, *J. Am. Chem. Soc.*, **88** 3209 (1966); J. A. Semlyen and P. V. Wright, *Polymer*, **10**, 543 (1969); M. S. Beevers and J. A. Semlyen, *ibid.*, **13**, 385 (1972); P. V. Wright, *J. Polym. Sci.*, **11**, 51 (1973).
(7) J. M. Andrews, F. R. Jones, and J. A. Semlyen, *Polymer*, **15**, 420 (1974).
(8) D. R. Cooper and J. A. Semlyen, *Polymer*, **14**, 185 (1973).
(9) P. J. Flory, *Pure Appl. Chem., Macromolecular Chem.*, **8**, 1–15 (1972).
(10) R. L. Jernigan and P. J. Flory, *J. Chem. Phys.*, **50**, 4165 (1969).
(11) D. Y. Yoon, results in preparation for publication.
(12) P. J. Flory, *Proc. Natl. Acad. Sci. U.S.A.*, **70**, 1819–1823 (1973).
(13) P. J. Flory and D. Y. Yoon, *J. Chem. Phys.*, **61**, 5358–5365 (1974).
(14) D. Y. Yoon and P. J. Flory, *J. Chem. Phys.*, **61**, 5366–5380 (1974).
(15) H. J. M. Bowen and L. E. Sutton, "Tables of Interatomic Distances and Configurations in Molecules and Ions", The Chemical Society, London, 1958; "Supplement", 1965.
(16) P. J. Flory, V. Crescenzi, and J. E. Mark, *J. Am. Chem. Soc.*, **86**, 146 (1964).
(17) P. J. Flory, *Macromolecules*, **7**, 381–392 (1974).
(18) J. C. Conrad and P. J. Flory, *Macromolecules*, following paper in this issue.
(19) G. Porod, *Monatsh. Chem.*, **80**, 259 (1949); O. Kratky and G. Porod, *Recl. Trav. Chim. Pays-Bas*, **68**, 1106 (1949).
(20) K. Nagai, *J. Chem. Phys.*, **38**, 924 (1963); **48**, 5646 (1968); K. Nagai and T. Ishikawa, *ibid.*, **45**, 3128 (1966).
(21) P. J. Flory and Y. Abe, *J. Chem. Phys.*, **54**, 1351 (1971).